INTERNATIONAL JOURNAL OF HYDROGEN ENERGY 34 (2009) 6690–6704

Available at www.sciencedirect.com

ScienceDirect

journal homepage: www.elsevier.com/locate/he

Radiative heat transfer in enhanced hydrogen outgassing of glass

*Rei Kitamura, Laurent Pilon**

University of California, Los Angeles, Henry Samueli School of Engineering and Applied Science, Mechanical and Aerospace Engineering Department, 420 Westwood Plaza, Eng. IV 37-132, Los Angeles, CA 90095-1597, USA

ARTICLE INFO

Article history:
Received 15 March 2009
Received in revised form
24 May 2009
Accepted 27 May 2009
Available online 9 July 2009

Keywords:
Hydrogen storage
Photo-induced gas diffusion
Hollow glass microspheres
Outgassing

ABSTRACT

This paper explores the physical mechanisms responsible for experimental observations that led to the definition of "photo-induced hydrogen outgassing of glass". Doped borosilicate glass samples were placed inside an evacuated silica tube and heated in a furnace or by an incandescent lamp. It was observed that hydrogen release from the glass sample was faster and stronger when heated by an incandescent lamp than within a furnace. Here, sample and silica tube were modeled as plane-parallel slabs exposed to furnace or to lamp thermal radiation. Combined conduction, radiation, and mass transfer were accounted for by solving the one-dimensional transient mass and energy conservation equations along with the steady-state radiative transfer equation. All properties were found in the literature. The experimental observations can be qualitatively explained based on conventional thermally activated gas diffusion and by carefully accounting for the participation of the silica tube to radiation transfer along with the spectral properties of the silica tube and the glass samples. In brief, the radiation emitted by the incandescent lamp is concentrated between 0.5 and 3.0 μm and reaches directly the sample since the silica tube is nearly transparent for wavelengths up to 3.5 μm. On the contrary, for furnace heating at 400 °C, the silica tube absorbs a large fraction of the incident radiation which reduces the heating rate and the H_2 release rate. However, between 0.8 and 3.2 μm undoped borosilicate does not absorb significantly. Coincidentally, Fe_3O_4 doping increases the absorption coefficient and also reacts with H_2 to form ferrous ions which increase the absorption coefficient of the sample by two orders of magnitude. Thus, doped and reacted samples heat up much faster when exposed to the heating lamp resulting in the observed faster response time and larger H_2 release rate.

1. Introduction

Hydrogen storage is arguably one of the main technological challenges for a viable hydrogen economy. Indeed, hydrogen reacts explosively with oxygen above the ignition temperature between 773 and 850 K at atmospheric pressure in air [1]. The criteria for choosing a hydrogen storage technology include (1) safety, (2) large volumetric and gravimetric energy densities, (3) fast loading and unloading, (4) numerous loading/unloading cycles, (5) low fabrication cost, and (6) low energy requirements for loading and unloading. For example, the hydrogen storage system for automotive applications should enable vehicle autonomy greater than 300 miles, safe operation under all circumstances including road accidents, fast refuelling, and on-demand availability. Numerous techniques have been proposed including (i) high pressure storage tanks at room

* *Corresponding author*. Tel.: +1 310 206 5598.
E-mail address: pilon@seas.ucla.edu (L. Pilon).
0360-3199/$ – see front matter
doi:10.1016/j.ijhydene.2009.05.113

Nomenclature

c_p	Specific heat at constant pressure, J/kg.K
C	Gas molar concentration, mol/m^3
D	Diffusion coefficient, m^2/s
D_0	Pre-exponential factor in Arrhenius, law, m^2/s
E_a	Activation energy, J/mol
$E_{b,\lambda}$	Spectral blackbody emissive power, W/m^2.μm
$f(\lambda T)$	Blackbody radiation function
I_λ	Spectral radiation intensity, W/m^2.sr.μm
$I_{b,\lambda}$	Blackbody radiation intensity, W/m^2.sr.μm
$I_{0,\lambda}$	Incident spectral intensity, W/m^2.sr.μm
k_c	Thermal conductivity, W/m.K
k	Absorption index
K	Permeability, mol/Pa.m.s
L	Slab thickness, m
M	Molar mass, g/mol
m	Complex index of refraction, $n - ik$
n	Slab refractive index
q_R	Radiative heat flux, W/m^2 or W/m^2.μm
$\dot{r}_{H_2}$	Reaction rate between H_2 and borosilicate glass, mol/m^3.s
R	Gas release rate, kg/s
S	Solubility in borosilicate glass, mol/m^3.Pa
t	Time, s
T	Temperature, K
T_f	Furnace temperature, K
T_ℓ	Incandescent lamp temperature, K
z	Location in the slab, m

Greek symbols

ϵ_λ	Spectral hemispherical emissivity
ϵ	Total hemispherical emissivity
θ	Polar angle
θ_{cr}	Critical polar angle
κ	Absorption coefficient, 1/m
λ	Wavelength of the incident radiation, m
λ_c	Cutoff wavelength of borosilicate sample, m
$\lambda_{c,t}$	Cutoff wavelength of silica tube, m
λ_{max}	Peak emission wavelength, m, $\lambda_{max}T = 2898$ μm.K
μ	Director cosine of the transmitted angle, $\mu = \cos\theta$
ρ	Slab density, kg/m^3
ρ_λ	Specular spectral reflectivity
σ	Stefan–Boltzmann constant, $\sigma = 5.67 \times 10^{-8}$ W/m^2.K^4
τ	Transmittance of an interface

Subscripts

0	Refers to values at $z = 0$
f	Refers to furnace heating
H_2	Refers to hydrogen
i	Refers to initial conditions
ℓ	Refers to lamp heating
L	Refers to values at $z = L$
sur	Refers to surrounding
t	Refers to silica tube
λ	Refers to wavelength-dependent quantity

temperature, (ii) liquid hydrogen containers at cryogenic temperatures (20 K), (iii) carbon nanotubes, (iv) metal hydrides, (v) microporous metal-organic framework, and (vi) hollow glass microsphere (HGMs) [2]. Unfortunately, none of the current technologies meet the 2015 performance and cost targets set by the US Department of Energy by a wide margin [3].

Hydrogen storage in HGMs presents the following advantages over other technologies. First, HGMs have large gravimetric energy. They are easy to handle at atmospheric pressure and ambient temperature and can be stored in any tank solution [2]. The technology is inexpensive, safe, and requires low energy consumption for production. The procedure for hydrogen storage and unloading in and out of HGMs consists of loading the hydrogen in the glass microspheres by placing them in a high temperature and high pressure hydrogen environment to accelerate gas diffusion inside the microspheres. Then, the hollow microspheres are quenched so that hydrogen remains trapped inside thanks to significant reduction in the H_2 diffusion coefficient through the shell. The stored hydrogen is released on demand by heating the hollow glass microspheres. However, major challenges face storage in HGMs including [2,4] (a) the low volumetric energy density, (b) the slow hydrogen release rate, (c) the need to heat the HGMs at temperatures above the operating temperature of polymer electrolyte membrane fuel cells, (d) the large amount of energy required to compress hydrogen to very high pressures used during H_2 loading (25% of storage energy [5]), and (e) manufacturing processes able to produce HGMs with controllable size and shell thickness capable of sustaining high pressures.

Recently, Shelby and co-workers [6–9] presented experimental study of what they called ''photo-induced hydrogen outgassing'' from borosilicate glass doped with various metal oxides especially Fe_3O_4 which is a mixture of FeO and Fe_2O_3 states. The authors observed that hydrogen release from a slab of doped borosilicate glass placed in a vitreous silica tube is accelerated when exposed to an incandescent heating lamp compared with heating in a furnace at 400 °C. The infrared lamp was a reflector type lamp (R-type) with peak emission around 1.3 μm. Similar results were recently obtained with cobalt-doped hollow glass microspheres loaded with hydrogen [10]. The authors suggested that ''*infrared radiation is contributing the activation energy necessary for hydrogen diffusion*'' [8]. To the best of our knowledge, this would constitute a new physical phenomenon. It remains unclear, however, how the total irradiance and the spectral nature of radiation would be accounted for in an Arrhenius type of relation for the diffusion coefficient given by $D = D_0 exp(-E_a/RT)$ where E_a is the activation energy of diffusion and D_0 is an empirical constant. Moreover, the reported experimental data do not isolate the proposed mechanism from the well known thermally activated gas diffusion. Recently, Zhevago and Glebov [11] suggested that illumination of the Fe_3O_4 doped borosilicate ''*causes the dopant to react thus opening microscopic pores that occur naturally in the glass*''. However, no direct observation of the suggested pores was provided. Regardless, the following experimental observations were made [6–9]: (a) the H_2 release from borosilicate glass samples was slower during furnace heating than heating

lamp except for undoped samples, (b) the onset of outgassing was observed immediately with lamp heating but was slower for furnace heating, (c) increasing the lamp intensity accelerated the H_2 release rate and the overall mass released from the sample, (d) borosilicate glass CGW 7070 demonstrated the best H_2 release response, (e) increasing the Fe_3O_4 doping level increases the H_2 release rate, (f) the steady-state sample temperature of 2 wt.% Fe_3O_4 doped borosilicate glass reached 472 °C for lamp heating while it was 400 °C for furnace heating, and (g) unlike for undoped borosilicate glass, hydrogen and deuterium outgassing was larger than that of helium for doped borosilicate.

The first mechanism for hydrogen dissolution in glass consists of physical dissolution when H_2 molecules occupy the interstices of the glass. The second mechanism involves chemical reactions between H_2 and the glass resulting in the formation of OH groups. For example, hydrogen causes the reduction of variable-valence ions such as Fe^{3+}, Ce^{4+}, and Sn^{4+} [12]. In particular, Fe^{3+} can be reduced almost completely to Fe^{2+} according to the reaction [12],

$$H_2 + 2(\equiv Si - 0)^- + 2Fe^{3+} \rightleftharpoons 2(\equiv Si - 0H) + 2Fe^{2+} \quad (1)$$

The reaction rate is much faster than the diffusion rate. Thus, the process is diffusion limited and can be accounted for through standard mass diffusion model with some effective diffusion coefficient, permeability, and solubility [13].

In soda-lime silicate glass, Johnston and Chelko [12] established that reduction of Fe^{3+} by H_2 into Fe^{2+} results in significant increase in the absorptance of the glass sample in the spectral range from 0.4 to 2.5 μm. The changes were apparent with the unaided eye. Similarly, Shelby and Vitko [14] observed (i) an increase in absorptance beyond 0.8 μm and (ii) a reduction in absorptance between 0.4 and 0.8 μm for soda-lime silicate. Rapp [9] confirmed Shelby and Vitko's results for Fe_3O_4 doped borosilicate glass showing an increase in the Fe^{2+}/Fe^{3+} ratio as the duration of exposure to hydrogen gas increases [8]. This was attributed to the fact that the absorption band around 380 nm corresponds to the ferric state (Fe^{3+}) while a peak around 1.1 μm corresponds to the ferrous state Fe^{2+}. In addition, the formation of OH groups results in a strong absorption band at wavelengths around 2.73–2.85 μm, 3.5 μm, and 4.5 μm [8,15,16].

The objectives of this study is to gain insight into the physical phenomena responsible for the experimental observations by Shelby and co-workers [6–9]. To do so, it investigates unloading of hydrogen stored in plane-parallel borosilicate glass slabs with different thicknesses and doping levels by modeling transient heat, radiation, and mass transfer for both furnace and incandescent lamp heating. The study also provides a tool to analyze experimental data and retrieve transport properties. The transport processes are described using conventional approaches and concepts as well as properties reported in the literature.

2. Analysis

Let us considered a plane-parallel slab of thickness L made of borosilicate glass placed in vacuum as illustrated in Fig. 1 along with the coordinate system. At time $t = 0$, the slab is exposed to thermal radiation provided either by an electric furnace preheated at temperature T_f or by a heating lamp emitting in the visible and near infrared parts of the electromagnetic spectrum. The slab is enclosed in an evacuated vitreous silica tube to impose approximately vacuum conditions. As a result of heating, the hydrogen gas physically dissolved previously in the slab diffuses out.

2.1. Assumptions

To make the problem mathematically trackable the following assumptions are made:

1. The heat, mass, and radiation transfer are treated as one-dimensional.
2. The slab is treated as homogeneous and isotropic for all optical and transport phenomena.
3. The material is in local thermodynamic equilibrium for which Planck's and Kirchhoff's laws are valid.
4. The slab thickness is much larger than the wavelength of radiation so coherent effects are negligible.
5. The slab is absorbing, emitting, but non-scattering.
6. The optical properties of the sample and of the silica tube remain unchanged while being exposed to the external radiation and as the oxidation state of the glass changes due to hydrogen outgassing.
7. As a first order approximation, optical and radiation properties of the slabs are assumed to be independent of temperature. For example, the absorption coefficient of BK7 borosilicate glass reported by Kunc et al. [17] was nearly unchanged between 293 and 770 K except around 4.3 μm when it did not vary by more than 15%.
8. The slab surfaces are optically smooth and specularly reflecting.
9. The radiation intensity I_λ is independent of azimuthal angle and depends only on location z and polar angle θ (Fig. 1).
10. Hydrogen is weakly soluble in borosilicate glass so Henry's law is applicable.
11. Diffusion is considered to be a thermally activated process only.
12. The diffusion coefficient and solubility of hydrogen in borosilicate glass are independent of concentration and irradiance, and depend only on temperature T.
13. The density of hydrogen is constant and negligibly small compared with the density of the glass which itself is assumed to be constant.
14. The partial specific volume of hydrogen in the glass is negligible.
15. Fe_3O_4 and Fe_2O_3 dopings affect only the optical properties of the borosilicate glass but not the thermophysical properties such as density, thermal conductivity, specific heat, and diffusion coefficient.
16. Since the surface of the surrounding enclosure is much larger than that of the slab, incident radiation on the slab can be treated as blackbody radiation at temperature T_{sur}. In the case of furnace heating, the surrounding temperature is uniform and equal to the furnace temperature, i.e., $T_{sur} = T_f$.

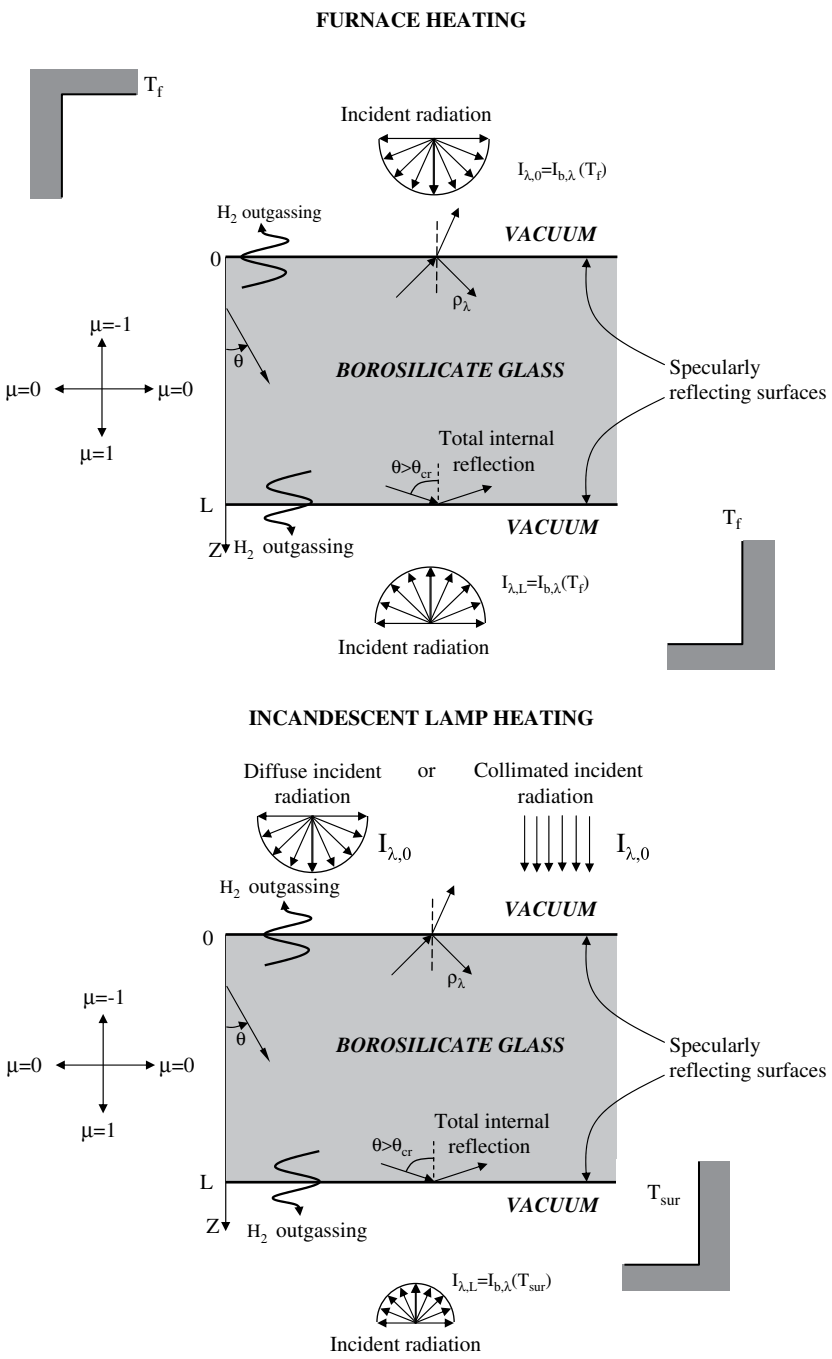

Fig. 1 – Schematic of the hydrogen outgassing from borosilicate glass slab by furnace and lamp heating.

2.2. *Governing equations for transient heat transfer*

As the incident radiation from the furnace wall or from the heat lamp is absorbed by the borosilicate glass sample, the temperature may not be uniform and combined conduction and radiation take place. Then, the transient one-dimensional energy conservation equation in terms of temperature $T(z, t)$ at location z and time t can be written as [18],

$$\rho c_p \frac{\partial T}{\partial t} = \frac{\partial}{\partial z}\left(k_c \frac{\partial T}{\partial z} - q_R(z)\right) \tag{2}$$

where ρ, c_p, and k_c are the density, specific heat, and thermal conductivity of the borosilicate glass slab, respectively. In addition, the local radiative heat flux $q_R(z)$ depends on the local spectral radiation intensity $I_\lambda(z, \mu)$ in a given direction θ and is expressed as [18],

$$q_{R,\lambda}(z) = 2\pi \int_{-1}^{1} I_\lambda(z,\mu)\mu d\mu \quad \text{and} \quad q_R(z) = \int_0^\infty q_{R,\lambda}(z) d\lambda \tag{3}$$

where $\mu = \cos\theta$ is the director cosine.

Moreover, the initial temperature is assumed to be uniform throughout the slab and is equal to T_i,

$$T(z,0) = T_i \quad \text{for } 0 \le z \le L \tag{4}$$

Two boundary conditions are also necessary for solving the energy conservation Equation (2). Radiation transfer is the only mode of heat transfer between the slab and its surrounding. Thus, the energy balance at both interfaces can be written as [19],

$$-k_c\frac{\partial T}{\partial z}|_{z=0} = -\epsilon(T_0)\sigma T_0^4 + \int_{\lambda_c}^{\infty}\epsilon_\lambda(T_0)q_{R,\lambda,0}d\lambda \quad \text{at } z=0 \tag{5}$$

$$-k_c\frac{\partial T}{\partial z}|_{z=L} = \epsilon(T_L)\sigma T_L^4 - \int_{\lambda_c}^{\infty}\epsilon_\lambda(T_L)q_{R,\lambda,L}d\lambda \quad \text{at } z=L \tag{6}$$

where T_0 and T_L are the slab temperatures at time t and location $z=0$ and $z=L$, respectively, i.e., $T_0 = T(z=0, t)$ and $T_L = T(z=L, t)$. Similarly, $q_{R,\lambda,0}$ and $q_{R,\lambda,L}$ are the spectral radiative heat fluxes incident on each side of the slab. The total hemispherical emissivity of borosilicate glass at temperature T is denoted by $\epsilon(T)$ and defined as [18],

$$\epsilon(T) = \frac{1}{\sigma T^4}\int_{\lambda_c}^{\infty}\epsilon_\lambda(T)E_{b,\lambda}(T)d\lambda \tag{7}$$

where $\epsilon_\lambda(T)$ is the spectral hemispherical emissivity and $E_{b,\lambda}(T)$ is the blackbody spectral emissive power given by Planck's law [18]. The cutoff wavelength λ_c corresponds to the wavelength beyond which borosilicate glass is opaque. According to Assumption 7, $\epsilon_\lambda(T)$ is independent of temperature but $\epsilon(T)$ depends on T through $E_{b,\lambda}(T)$.

The above boundary conditions are valid for any situation but simplify when the sample is heated within a furnace. Then, the radiative heat flux incident on both sides is the blackbody radiation intensity at the furnace temperature T_f, i.e., $q_{R,\lambda,0} = q_{R,\lambda,L} = \pi I_{b,\lambda}(T_f)$ where $I_{b,\lambda}(T)$ is the blackbody spectral intensity such that $E_{b,\lambda}(T) = \pi I_{b,\lambda}(T)$. Then, the above boundary conditions simplify to,

$$-k_c\frac{\partial T}{\partial z}|_{z=0} = -\epsilon(T_0)[1-f(\lambda_c T_0)]\sigma T_0^4 + \epsilon(T_0)\left[1-f\left(\lambda_c T_f\right)\right]\sigma T_f^4 \text{ at } z=0 \tag{8}$$

$$-k_c\frac{\partial T}{\partial z}|_{z=L} = \epsilon(T_L)[1-f(\lambda_c T_L)]\sigma T_L^4 - \epsilon(T_L)\left[1-f\left(\lambda_c T_f\right)\right]\sigma T_f^4 \text{ at } z=L. \tag{9}$$

$$\rho_\lambda(\mu) = \begin{cases} \frac{1}{2}\left[\left(\frac{\mu - n_\lambda\sqrt{1-n_\lambda^2(1-\mu^2)}}{\mu + n_\lambda\sqrt{1-n_\lambda^2(1-\mu^2)}}\right)^2 + \left(\frac{n_\lambda\mu - \sqrt{1-n_\lambda^2(1-\mu^2)}}{n_\lambda\mu + \sqrt{1-n_\lambda^2(1-\mu^2)}}\right)^2\right] & \text{for } 0 \le \theta \le \theta_{cr} \\ \frac{1}{2}\left[\left(\frac{-\mu - n_\lambda\sqrt{1-n_\lambda^2(1-\mu^2)}}{-\mu + n_\lambda\sqrt{1-n_\lambda^2(1-\mu^2)}}\right)^2 + \left(\frac{-n_\lambda\mu - \sqrt{1-n_\lambda^2(1-\mu^2)}}{-n_\lambda\mu + \sqrt{1-n_\lambda^2(1-\mu^2)}}\right)^2\right] & \text{for } \pi - \theta_{cr} \le \theta \le \pi \\ 1 & \text{for } \theta_{cr} \le \theta \le \pi - \theta_{cr} \end{cases} \tag{15}$$

The function $f(\lambda T)$ is the blackbody radiation function representing the fraction of the total blackbody emission in the spectral band from 0 to λ_c and expressed as [20],

$$f(\lambda_c T) = \frac{\int_0^{\lambda_c} E_{b,\lambda}(T)d\lambda}{\int_0^{\infty} E_{b,\lambda}(T)d\lambda} = \frac{\int_0^{\lambda_c} E_{b,\lambda}(T)d\lambda}{\sigma T^4}. \tag{10}$$

In this study, the values of $f(\lambda_c T_0)$ and $f(\lambda_c T_L)$ were computed at every time step.

2.3. Radiative transfer equation

The spectral intensity I_λ necessary to compute the heat flux $q_{R,\lambda}(z)$ satisfies the steady-state one-dimensional radiation transfer equation (RTE) for an absorbing, emitting, but non-scattering medium expressed as [18],

$$\mu\frac{dI_\lambda(z,\mu)}{dz} = \kappa_\lambda\left[n_\lambda^2 I_{b,\lambda}(T(z,t)) - I_\lambda\right] \tag{11}$$

where n_λ is the refractive index of the glass slab. The term $n_\lambda^2 I_{b,\lambda}(T(z,t))$ represents the blackbody radiation emitted by the slab at location z. The absorption coefficient κ_λ is defined as,

$$\kappa_\lambda = \frac{4\pi k_\lambda}{\lambda} \tag{12}$$

where k_λ is the imaginary part of the complex index of refraction of the slab denoted by $m_\lambda = n_\lambda - ik_\lambda$. The RTE is expressed on a spectral basis because the radiation and optical properties of borosilicate glass strongly depend on wavelength.

Both faces of the slab are assumed to be optically smooth and specularly reflecting. Thus, the boundary conditions for solving the RTE can be written as [19,21],

$$I_\lambda(0,\mu) = \tau_\lambda(\mu)n_\lambda^2 I_{\lambda,0} + \rho_\lambda(\mu)I_\lambda(0,-\mu) \quad \text{for } \mu \ge 0 \tag{13}$$

$$I_\lambda(L,\mu) = \tau_\lambda(\mu)n_\lambda^2 I_{\lambda,L} + \rho_\lambda(\mu)I_\lambda(L,\mu) \quad \text{for } \mu \le 0 \tag{14}$$

where, $I_{\lambda,0}$ and $I_{\lambda,L}$ denote the radiation intensities incident on each face of the sample. Furthermore, the reflectivity and transmissivity of the borosilicate glass/vacuum interface are denoted by $\rho_\lambda(\mu)$ and $\tau_\lambda(\mu) = 1 - \rho_\lambda(\mu)$, respectively. Note that the radiation incident on the slab/vacuum interface coming from within the slab is internally reflected for incidence angles larger than the critical angle θ_{cr} defined as $\sin\theta_{cr} = 1/n_\lambda$. The reflectivity is given by Fresnel's equation [19,21],

The values of $I_{\lambda,0}$ and $I_{\lambda,L}$ depend on the heating method. When the sample is heated within the furnace at temperature T_f, both faces are subject to diffuse incident radiation intensities $I_{\lambda,0}$ and $I_{\lambda,L}$ equal to the blackbody spectral intensity $I_{b,\lambda}(T_f)$,

$$I_{\lambda,0} = I_{\lambda,L} = I_{b,\lambda}\left(T_f\right). \tag{16}$$

On the other hand, lamp heating is performed with a typical reflector incandescent heat lamp whose radiation is emitted by a tungsten filament at temperature T_ℓ [22]. To be able to compare the hydrogen release rates from furnace heating with that from lamp heating, the same incident heat flux was imposed in both heating methods. The total irradiance on both sides of the sample from the furnace is equal to $q = q_{R,0} + q_{R,L} = 2\sigma T_f^4$. Thus, for diffuse incident radiation from the lamp, the boundary conditions for the spectral intensity is expressed as,

$$I_{\lambda,0}(z=0,\mu) = 2\left(\frac{T_f}{T_\ell}\right)^4 I_{b,\lambda}(T_\ell) \quad \text{for } 0 \le \mu \le 1. \tag{17}$$

The factor 2 appears because furnace heating takes place from both sides of the slab while lamp heating is incident only on one side (Fig. 1). Similarly, for collimated incidence, the boundary condition is expressed as,

$$I_{\lambda,0}(z=0,\mu) = 2\pi\left(\frac{T_f}{T_\ell}\right)^4 I_{b,\lambda}(T_\ell)\delta(\mu-1) \quad \text{for } 0 \le \mu \le 1 \tag{18}$$

where, $\delta(x)$ is the Dirac delta function. The above boundary conditions for lamp heating ensure that the incident radiation is proportional to the blackbody spectral distribution at temperature T_ℓ with maximum emission wavelength λ_{max} such that $\lambda_{max}T_\ell = 2898$ μm.K while keeping the overall incident heat flux equal to that of a furnace at 400 °C. The other side of the sample exchanges radiation with the surroundings at temperature T_{sur}, i.e.,

$$I_{\lambda,L}(z=L,\mu) = I_{b,\lambda}(T_{sur}) \quad \text{for } -1 \le \mu \le 0. \tag{19}$$

In all the simulations for lamp heating T_{sur} was assumed to be equal to 25 °C.

Note that the goal of this parametric study was not to model precisely the lamp emission intensity since its absolute spectral intensity along with other experimental conditions were not reported. Instead, the lamp was treated as a blackbody source and the temperature of its filament T_ℓ was varied to assess the effect of the spectral distribution of the incident intensity. The spectral intensity predicted by Equations (17) and (18) for $T_\ell = 1700$ K, 2300 K, and 2900 K covers the spectral range where the emission intensity of the heating lamp used by Rapp [9] is concentrated (see Supplemental Materials).

2.4. Mass conservation equation

The unloading of the hydrogen gas dissolved in the borosilicate glass slab by physical diffusion is governed by the transient one-dimensional mass conservation equation expressed as,

$$\frac{\partial C_{H_2}}{\partial t} = \frac{\partial}{\partial z}\left(D_{H_2}(T)\frac{\partial C_{H_2}}{\partial z}\right) + \dot{r}_{H_2} \tag{20}$$

where, C_{H_2} is the molar concentration of H_2 in the slab expressed in mol/m^3 while $D_{H_2}(T)$ is the diffusion coefficient of hydrogen through borosilicate glass expressed in m^2/s. Note that $D_{H_2}(T)$ is a function of temperature which depends on location z in the slab. The reaction rate between hydrogen and the borosilicate glass is denoted by $\dot{r}_{H_2}$. Even though hydrogen reacts with doped borosilicate glass, the reaction is diffusion limited at the temperatures considered in this study. Thus, reaction rate(s) are negligible compared with the hydrogen diffusion rate and only the diffusion term on the right-hand side of Equation (20) is considered. Moreover, the chemical solubility of hydrogen can be accounted for as physical solubility. Thus, physical hydrogen dissolution and diffusion are assumed to be the dominant mechanisms of hydrogen outgassing [23] as established experimentally (see Ref. [9], Fig. 4.2, p. 78).

The initial concentration of hydrogen $C_{H_2,i}$ is assumed to be uniform across the slab. It is computed under the assumption that hydrogen was dissolved in the slab in pure hydrogen atmosphere at temperature T_{load} and pressure p_{load} so that

$$C_{H_2}(z, t=0) = C_{H_2,i} = S_{H_2}(T_{load}, p_{load})p_{load} \tag{21}$$

where $S_{H_2}(T_{load}, p_{load})$ is the solubility of hydrogen in borosilicate glass expressed in mol/m^3.Pa. The loading temperature T_{load} and pressure p_{load} are taken as 500 °C and 1 bar, respectively, as used experimentally by Rapp and Shelby [8]. The two boundary conditions needed to solve the mass conservation equation assumes that the slab is surrounded by vacuum at all time so that,

$$C_{H_2}(0,t) = C_{H_2}(L,t) = 0 \quad \text{for } t > 0. \tag{22}$$

2.5. Lump system approach

When the slab is thin enough, the temperature is uniform throughout and heat conduction need not be considered. Then, the lumped system approach can be used to predict the evolution of the sample temperature $T(t)$ as a function of time. In the case of furnace heating, the energy conservation equation is written as,

$$\rho c_p L\frac{dT}{dt} = 2\epsilon(T)\left[1 - f(\lambda_c T_f)\right]\sigma T_f^4 - 2\epsilon(T)[1 - f(\lambda_c T)]\sigma T^4 \tag{23}$$

where the first term on the right-hand side of Equation (23) corresponds to the absorption of the radiation from the furnace while the second corresponds to emission by the sample. The factor 2 accounts for irradiation and emission from both faces of the sample.

2.6. Simulating experimental conditions

Experiments of hydrogen outgassing from borosilicate glass samples with various compositions and doping elements and concentrations were conducted by Shelby and co-workers [6–9]. In their experiments, the hydrogen release rate was estimated by measuring the hydrogen partial pressure using mass spectrometry. An additional difficulty in comparing experimental data with numerical simulations lies in the fact that the sample was enclosed in a silica tube which absorbs part of the furnace radiation and in turn exchange radiation with the sample. Moreover, the samples used experimentally were 1 mm thick and had a surface area of 1×1 cm^2.

In the present study and as a first order approximation, the sample was simulated as enclosed between two semi-infinite plane-parallel silica slabs of thickness L_t at temperature T_t. One-dimensional heat, mass, and radiation transfers were considered. The temperatures of the sample and of the silica tube were simulated using the lump system approach. The

sample temperature T satisfy the following energy conservation equation,

$$\rho c_p L\frac{dT}{dt} = 2\epsilon\left\{\left[f(\lambda_{c,t}T_f) - f(\lambda_c T_f)\right]\sigma T_f^4 - [f(\lambda_{c,t}T) - f(\lambda_c T)]\sigma T^4\right\} + 2\frac{[1-f(\lambda_{c,t}T_t)]\sigma T_t^4 - [1-f(\lambda_{c,t}T)]\sigma T^4}{1/\epsilon_t + 1/\epsilon - 1}. \quad (24)$$

The first term on the right-hand side represents the radiation exchange between both faces of the sample and the furnace for wavelengths between λ_c and $\lambda_{c,t}$. The second term accounts for the radiation exchange between the silica tubes and the sample faces for wavelengths beyond the silica cutoff $\lambda_{c,t}$. The emissivities of the silica tube and of the sample are assumed to be independent of temperature and wavelength beyond their respective cutoff wavelengths.

Each silica slab exchanges with the furnace at temperature T_f and the sample inside at temperature T. Thus, energy conservation equation for each silica slab having temperature T_t is expressed as,

$$\rho_t c_{p,t} L_t\frac{dT_t}{dt} = \epsilon_t\left\{[1-f(\lambda_{c,t}T_f)]\sigma T_f^4 - [1-f(\lambda_{c,t}T_t)]\sigma T_t^4\right\} + \frac{[1-f(\lambda_{c,t}T)]\sigma T^4 - [1-f(\lambda_{c,t}T_t)]\sigma T_t^4}{1/\epsilon_t + 1/\epsilon - 1}. \quad (25)$$

The first term on the right-hand side represents the radiation exchange between the outer surface of the tube and the furnace walls. The second accounts for the radiative heat transfer between the silica tube inside surface and the sample treated as gray diffuse plane-parallel slabs.

Moreover, the total heat input during furnace heating is given by $q_R = 2\sigma T_f^4$ with $T_f = 673$ K corresponding to 2.33 W/cm^2. In presence of silica tube, the heat flux reaching the sample is reduced due to absorption by the silica tube before the latter reaches the furnace temperature. For lamp heating, Rapp [9] used two types of lamp namely Sylvania 250 W R40 and General Electric red "Chill chaser" 250 W R40 (Ref. [9], p. 92). Both had tungsten filament and R40 bulb type 12.7 cm (5 inches) in diameter with a built-in reflector. The nominal lamp wattage was 250 W at voltage 120 V. Dushcenko et al. [24] measured the irradiance distribution delivered by similar heating lamps. They measured a heat flux of 2.0 W/cm^2 incident on a surface placed 10 cm away along the axis of a 250 W heating lamp. During hydrogen outgassing experiments, Rapp and Shelby [8] placed the samples 1 cm away from the lamp. Moving the sample away from the lamp reduced the irradiance [24] and the hydrogen release rate [7,9]. In other words, commercial 250 W R40 incandescent heating lamps can easily match or exceed the heat flux delivered by a furnace around 400 °C.

2.7. Constitutive relationships

The thermophysical properties of borosilicate glass required to solve the above governing equations for heat, radiation, and mass transfer are (i) the thermal conductivity $k_c(T)$, (ii) the product of the specific heat $c_p(T)$ and the density $\rho(T)$, (iii) the diffusion coefficient $D_{H_2}(T)$, (iv) the solubility $S_{H_2}(T,p)$, (v) the real and imaginary parts of the complex index of refraction of borosilicate glass n_λ and k_λ, (vi) the spectral hemispherical emissivity $\epsilon_\lambda(T)$, and (vii) the cutoff wavelengths λ_c and $\lambda_{c,t}$. Special attention was paid to Fe_3O_4 doped borosilicate glass CGW 7070 which experimentally exhibited superior hydrogen release response [8]. CGW 7070 performances were followed closely by those of CGW 7740 [8]. Unlike CGW 7070, the thermophysical properties of borosilicate glass CGW 7740 are readily available in the literature and were used in this study. Note that the composition of CGW 7070 and CGW 7740 differ in terms of SiO_2 and B_2O_3 contents with 72 wt.% and 25 wt.% for CGW 7070 compared with 81 wt.% and 13 wt.% for CGW 7740, respectively. As a first order approximation, these differences were assumed to have no significant effects on $k_c(T)$, $c_p(T)$, $\rho(T)$, $D_{H_2}(T)$, and $S_{H_2}(T,p)$. However, optical properties of undoped, 0.5 wt.%, and 2 wt.% Fe_3O_4 doped CGW 7070 were retrieved from transmittance data of samples saturated under 0.94 atm. and 500 °C as reported by Rapp [9] and using Eq. (14) in Ref. [25].

The thermal conductivity and specific heat of borosilicate glass CGW 7740 for temperatures ranging from room temperature to 250 °C have been reported by Assael et al. [26]. The thermal conductivity $k_c(T)$ is given by [26],

$$k_c(T) = 1.15\left[0.7688 + 0.2158\left(\frac{T}{298.15}\right) + 0.0157\left(\frac{T}{298.15}\right)^2\right] \quad (26)$$

where, T is expressed in Kelvin. Note that the data agrees well with those reported by Johnson and Hasselman [27] for temperatures up to 550 °C.

Furthermore, Assael et al. [26] expressed the product of density ρ and specific heat c_p of CGW 7740 as,

$$\rho(T)c_p(T) = 1770\left[0.8716 + 0.1634\left(\frac{T}{298.15}\right) - 0.035\left(\frac{T}{298.15}\right)^2\right]. \quad (27)$$

Here also T is expressed in Kelvin. The correlation agrees with data reported by Richet et al. [28] for c_p alone at temperatures between 120 °C and 512 °C assuming a constant density of 2230 kg/m^3 [29].

Moreover, the diffusion coefficient and permeability of deuterium D_2 in borosilicate glass CGW 7740 have been reported by Shelby [30] over the temperature range from 25 to 560 °C. The results agree well with those measured by Laska et al. [31] for deuterium between 25 and 500 °C and by Altemose [32] for hydrogen from 200 to 600 °C [23]. Permeability of deuterium is slightly lower than that of hydrogen by virtue of the fact that the mass of D_2 is larger than that of H_2. This difference, however, is negligible compared with differences between different experimental studies for the same gas. Thus, data reported by Shelby [30] were used and are given by,

$$D_{H_2}(T) = 1.06\times10^{-10}\mathrm{Texp}\left(\frac{-5385}{T}\right) \quad \text{in m}^2/\text{s} \quad (28)$$

$$K_{H_2}(T) = 2.787\times10^{-17}\mathrm{Texp}\left(\frac{-4026}{T}\right) \quad \text{in mol/Pa.m.s} \quad (29)$$

$$S_{H_2}(T) = \frac{K_{H_2}(T)}{D_{H_2}(T)} = 2.62\times10^{-7}\exp\left(\frac{1359}{T}\right) \quad \text{in mol/m}^3\text{Pa} \quad (30)$$

where, T is expressed in Kelvin. In this study, it is assumed that those expressions can be used for hydrogen gas and for CGW 7070 doped with Fe_3O_4 as confirmed experimentally [9] (p. 277).

The complex index of refraction of borosilicate glass used in Equations (11)–(15) was reported by De Sousa Meneses et al. [33] at room temperature over the spectral range beyond 4.0 μm. It is assumed that the formula can be used for n_λ for wavelengths between 300 nm and 10 μm as suggested by the good match with data reported by Melles Griot Inc. [34] for borosilicate glass between 486 and 644 nm. On the other hand, the absorption index k_λ over the spectral range from 500 nm to 10 μm was reconstructed from (i) transmittance data between 500 nm and 3.5 μm reported by Rapp [9] for undoped and Fe_3O_4 doped CGW 7070 saturated with H_2, (ii) from Sahba and Rockett [35] between 3.5 and 4.5 μm, and (iii) from De Sousa Meneses et al. [33] for wavelengths larger than 4.5 μm. Overall, the data from these various sources agree well with each other and cover the useful wavelength range while capturing the effect of doping in the spectral region between 500 nm and 3.5 μm. The refractive and absorption indices of borosilicate glass used in this study are presented in Fig. 2.

Furthermore, experimental data reported in the literature [36] and summarized by Touloukian and DeWitt [37] indicates that the total normal emissivity of borosilicate glass is nearly independent of temperature (Ref. [37], p. 1540). In addition, the cutoff wavelength λ_c is estimated to be 3.5 μm beyond which the spectral hemispherical emissivity is assumed to be constant and equal to 0.85 [38], i.e., $\epsilon_\lambda(T) = 0.85$ for $\lambda \geq 3.5$ μm. This can be justified by the fact that the directional emissivity of glass varies very little over most of the hemisphere and decreases rapidly at grazing angles [18]. In addition, beyond 3.5 μm, the presence of Fe_3O_4 doping does not affect the absorption index of borosilicate glass as shown in Fig. 2.

Finally, the density of the silica tube ρ_t is assumed to be constant and equal to 2200 kg/m^3 [39] while its specific heat $c_{p,t}$ is given by [40],

$$c_{p,t}(T_t) = 1927.74 - \frac{1220.88}{(1 + 0.0042T_t)^{0.77}} \quad (31)$$

where, the temperature of the silica slab T_t is expressed in °C. In addition, the absorption index of silica glass from 0.3 to 10 μm reported in the literature [41–43] is also plotted in Fig. 2 based on the recent review by Kitamura et al. [25]. The transmittance of a 1 mm thick slab of silica is about 50% at 4.5 μm and decreases from about 90% around 3.6 μm to practically 0.0 at 4.85 μm according to theoretical calculations using optical properties reported by Drummond [41]. Thus, the silica slabs are treated as transparent for wavelengths lower than the cutoff wavelength $\lambda_{c,t} = 4.5$ μm. Beyond 4.5 μm, they absorb the furnace radiation and emits radiation at their own temperature. The total hemispherical emissivity of silica $\epsilon_t(T_t)$ at all temperatures is taken constant and equal to 0.8 as measured by Tanaka et al. [44].

2.8. *Method of solution*

The above equations must be solved numerically as (i) thermophysical properties depend on temperature, (ii) radiation and optical properties depend strongly on wavelength, and (iii) internal reflection must be accounted for. An implicit time-marching method was used to solve the energy and mass conservation Equations (2) and (20) based on finite

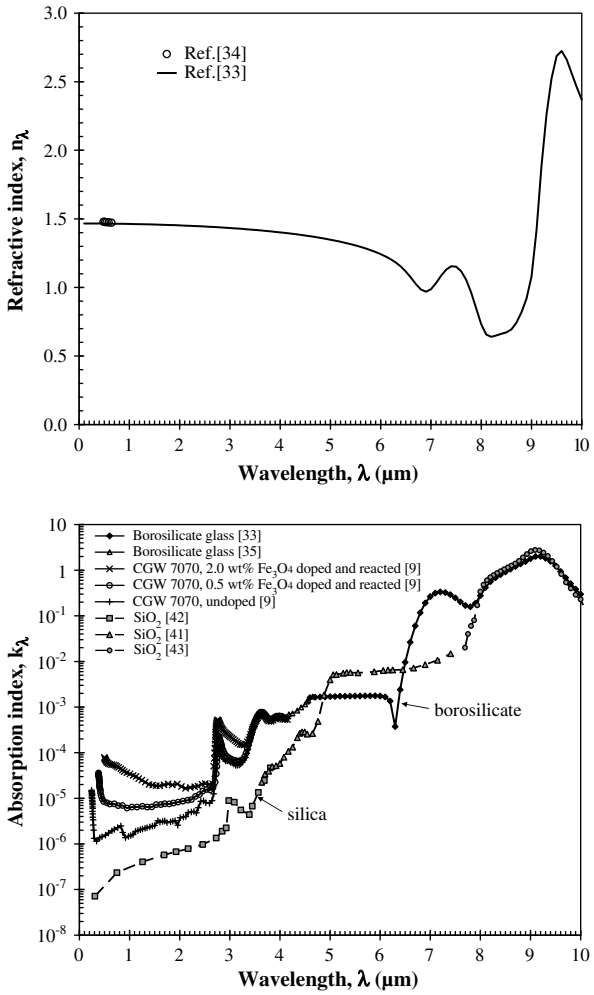

Fig. 2 – The refractive and absorption indices of undoped and Fe_3O_4 doped borosilicate glass obtained or retrieved from various sources [9,33,35,41,43,51].

volume method [45]. In addition, the RTE [Equation (11)] was solved numerically on a spectral basis using the discrete ordinates method [18,21] combined with finite volume method on a non-uniform grid. The integrals over solid angle were replaced by a weighted sum over discrete directions. In the present study, 8 directions per quadrant (S-8 approximation) were used and the weights were obtained from Ref. [18] (p. 503). The intensity was computed by an iterative method in which convergence criteria can be chosen arbitrarily. The spectrum between 500 nm and λ_c was discretized in N_λ wavelengths for both furnace and lamp heating with a spectral resolution of $\Delta\lambda = 0.1$ μm. The divergence of the local radiative heat flux q_R at time t was computed from the value of local spectral intensity $I_\lambda(z,\mu)$ at the previous time step. Spectral integration in Equations (3), (8), and (9) was performed using Simpson's rule for equally spaced wavelengths.

The grid used to compute both the radiation intensity and the radiative heat flux was staggered with that used for temperature and hydrogen concentration. The non-uniform grid was symmetric with respect to $z = L/2$ and formed with the smallest element at the boundaries $z = 0$ and $z = L$ where the initial concentration gradient was very large. The grid size

Δz_i for the ith finite volume was such that $\Delta z_i = r\Delta z_{i-1}$ where r is the size ratio between two adjacent cells and the smallest cell size is $\Delta z_0 = L(r-1)/2(r^{N/2}-1)$ where N is the even number of meshes. In all simulations r was taken as 1.1.

Numerical convergence was established by increasing the number of meshes by a factor 1.3 and dividing the time step by a factor 2. The results were considered to be converged when the relative differences in both the hydrogen release rate and the local temperature between two consecutive grid and time step refinements were less than 1%. The steady-state solution of the RTE was considered to be reached when the absolute difference between the values of intensity in all directions and at all wavelengths at the present and previous iteration was less than 10^{-5}. A numerically converged solution was obtained with $N_z = 130$ grid points, $N_\lambda = 31$ discrete wavelengths between 500 nm and λ_c, and time step $\Delta t = 0.25$ s.

The numerical code was successfully validated with analytical solutions and with numerical results reported in the literature. These include (1) transient and steady-state heat conduction without radiation [20], (2) absorbing but non-scattering gray slab with black surfaces subjected to diffuse or collimated incident radiation without heat conduction [18], (3) steady-state combined 1 D conduction and radiation in a slab between black surfaces at different temperatures [46]. Further validation was performed by comparing results for the full simulations with those for the lump system approach.

Finally, to enable comparison with experimental data, it is interesting to compute the hydrogen release rate. This required post-processing of the numerical results for $C_{H_2}(z,t)$. The residual mass of hydrogen in the slab per unit surface area at time t denoted by $m''_{H_2}(t)$ (in kg/m^2) and the associated hydrogen release rate denoted by $R_{H_2}(t)$ (in kg/m^{2}s), are defined, respectively as,

$$m''_{H_2}(t) = M_{H_2}\int_0^L C_{H_2}(z,t)dz \quad \text{and} \quad R_{H_2}(t) = -\frac{dm''_{H_2}}{dt} \tag{32}$$

where M_{H_2} is the hydrogen molar mass, $M_{H_2} = 2.016$ g/mol. The experimentally measured hydrogen partial pressure reported [8] is proportional to the hydrogen release rate R_{H_2}. Here, the numerical integration over the spatial coordinate z was performed using the trapezoidal rule for unequally spaced grids while the time derivative were computed numerically using the Newton forward difference polynomial [47].

3. Results and discussion

3.1. Furnace heating

In this section, parametric study investigating hydrogen release by furnace heating is discussed.

3.1.1. Lump system approach versus full simulations

In order to further assess the validity of the lump system approach for a slab of undoped borosilicate glass exposed to diffuse blackbody radiation emitted by the furnace, simulations were performed for furnace temperature of 400 °C and various sample thicknesses. First, Equations (2)–(11) along with the associated boundary conditions for furnace heating were solved numerically. The parameters used in the calculations were $T_i = 25$ °C, $T_f = 400$ °C as used experimentally by Kenyon [7] and Rapp and Shelby [8]. The temperature distribution in 1 and 10 mm thick undoped borosilicate slabs was compared (not shown) with predictions from the lump system approach. It indicates that temperature was nearly uniform throughout the 1 mm thick slab at all times and reaches steady state in about 90 s. Similar results were observed for slab thickness of 2.0 and 5.0 mm (not shown). However, non-uniform temperature was apparent in the 10 mm thick sample where steady state is reached after about 900 s. As previously discussed, the lump system approach assumes that the slab temperature is uniform across the slab thickness which seems to be the case for thin enough slabs.

Fig. 3 compares the evolution of the slab surface temperature as a function of time predicted by the lump system approach and by solving the coupled conduction and radiation equations (referred to as "full simulations"). It establishes that results obtained from the two methods agree very well for slab thickness L strictly smaller than 10 mm. The maximum relative difference between the two approaches varies from 7.7% for 1 mm thick sample to 37% for 10 mm thick sample. Therefore, for furnace heating and thin enough samples, the lump system approach gives accurate results and can be used with confidence. This approach presents the advantage of solving a non-linear ordinary differential equation and offers a simpler alternative to the coupled partial differential equations for conduction and radiation [Equations (2) and (11)].

Moreover, Fig. 4 shows the hydrogen concentration distribution $C_{H_2}(z,t)$ in a 1 mm thick undoped borosilicate slab at different times. It indicates that the hydrogen concentration in the slab is highly non-uniform and large concentration gradients exist near the boundaries; particularly at early stages of the outgassing process.

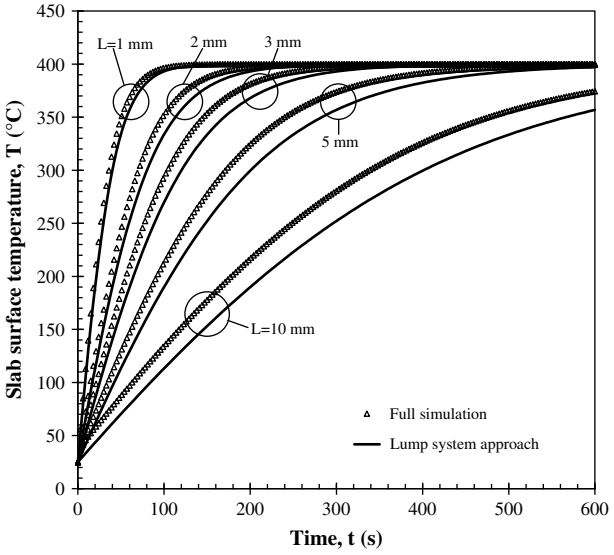

Fig. 3 – Temporal evolution of the temperature at the slab surface for different sample thicknesses predicted by (a) solving Equations (2)–(20) (full simulations) and (b) lump system approach [Equation (23)].

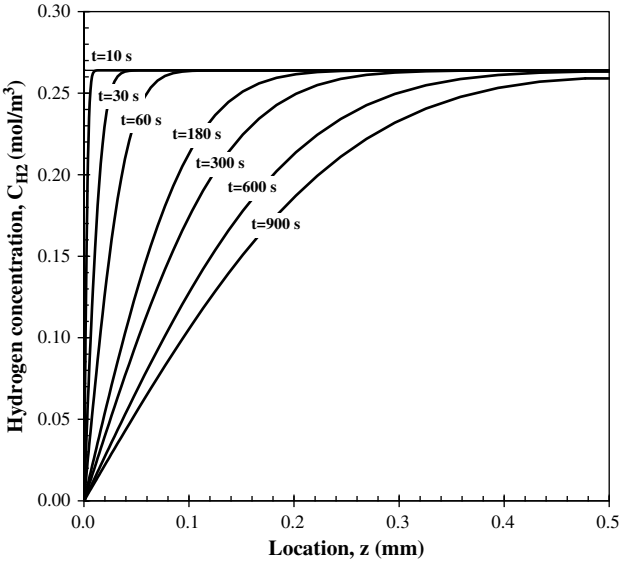

Fig. 4 – Concentration distribution of H_2 in a 1-mm thick undoped borosilicate sample in a furnace at $T_f = 400$ °C. Only half of the slab is shown.

3.1.2. *Effect of furnace temperature and sample optical properties*

First, the effect of furnace temperature T_f on the hydrogen outgassing is assessed by considering three values of T_f namely 400, 500, and 600 °C for the 1 mm thick slab. Fig. 5 shows the temporal evolution of the (i) slab temperature, (ii) residual hydrogen mass in the slab $m''_{H_2}(t)$, and (iii) hydrogen release rate $R_{H_2}(t)$ as a function of time for a 1 mm thick undoped sample. As expected, the heating rate and final temperature of the slab as well as the hydrogen release rate increase with the furnace temperature. The temperature reaches 99% of its steady-state value of T_f relatively rapidly within 60–100 s. In addition, the hydrogen release rate reaches a maximum at approximately the same time after 30–55 s for the three furnace temperatures considered. However, it takes about 3 h 18 min, 1 h, and 27 min for 95% of the loaded hydrogen to entirely diffuse out of the sample for furnace temperature T_f of 400, 500, and 600 °C, respectively. The same trends were observed for thicker slabs (not shown). It is interesting to note that the maximum release rate is reached much faster than observed experimentally [8] when the samples were inserted in an evacuated silica tube and placed in the furnace as explained later.

Moreover, as noted earlier, the absorption coefficient of the Fe_3O_4-doped borosilicate glass increases in the spectral region from 0.8 to 3.5 μm during hydrogen loading. Then, the absorption coefficient k_λ can reach up to 5×10^{-4} for 2 wt.% Fe_3O_4 doping [9]. Thus, the effect of the sample absorption coefficient (i.e., doping concentration) was assessed by varying the value of k_λ assumed to be constant between 0.8 and 3.5 μm with values between 0.0 and 5×10^{-4}. The maximum relative difference was 1.26% for the sample temperature and 1.76% for the hydrogen release rate during furnace heating at 400 °C. In other words, Figs. 3 and 4 are valid for all doping levels. This can be explained by the fact that the furnace spectral emissive

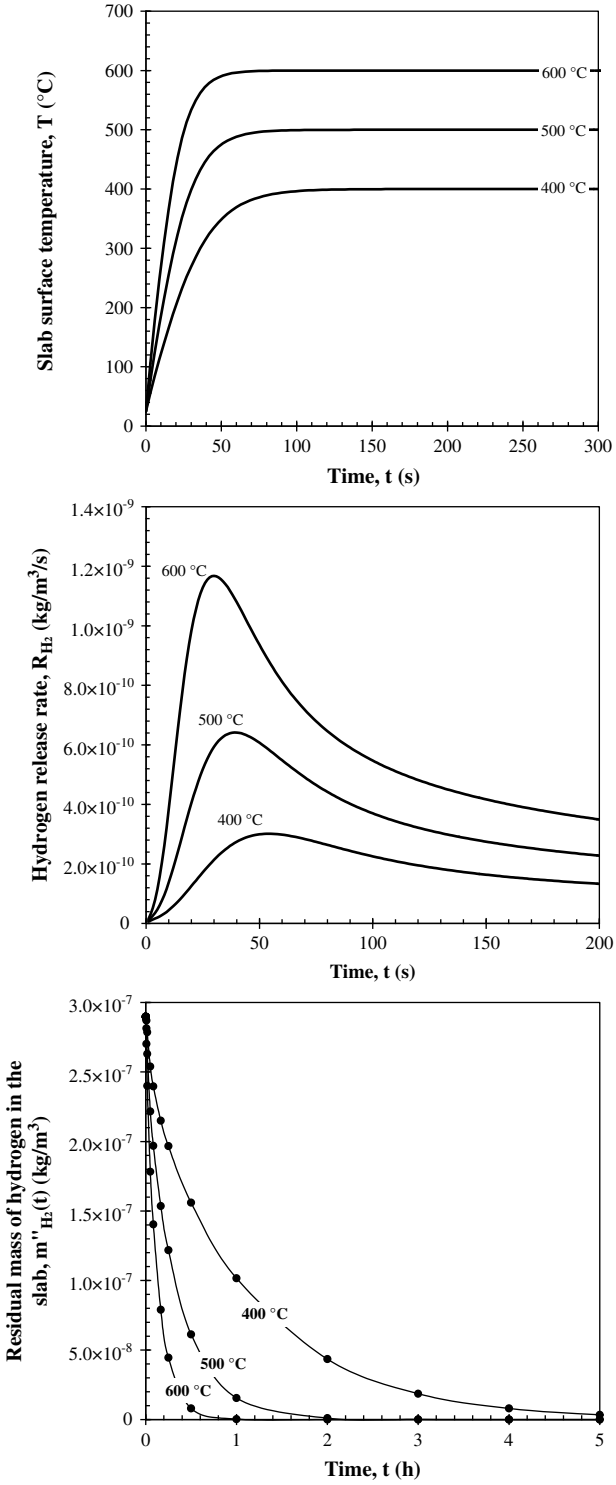

Fig. 5 – Temporal evolution of the temperature $T(t)$, residual mass $m''_{H_2}(t)$, and H_2 release rate $R_{H_2}(t)$ of a 1-mm thick undoped borosilicate sample in a furnace at temperatures $T_f = 400$ °C, 500 °C, and 600 °C.

power reaches a maximum at wavelength λ_{max} given by Wien's displacement law, $\lambda_{max}T_f = 2898$ μm.K. For a furnace temperature of $T_f = 400$ °C, $\lambda_{max} = 4.3$ μm and about 87% of the total emissive power is emitted at wavelengths larger than 3.5 μm. Thus, the effect of iron doping of borosilicate glass on sample

temperature and hydrogen outgassing during furnace heating is negligible. Similar qualitative observations were made experimentally [8].

3.2. *Incandescent lamp heating*

This section discussed the effects of parameters controlling radiation emitted by the incandescent lamp on the sample temperature and on the hydrogen release rate along with the effect of the Fe_3O_4 doping level. Note that the effect of the total emissive power is obvious: as the total irradiance increases, the temperature and the hydrogen release rate increases. This was observed experimentally by increasing the lamp voltage [8]. It will not be considered further in order to focus on less intuitive effects. In fact, all simulations assessing the effect of diffuse versus collimated incident radiation and of the lamp emission spectrum were performed for the same heat input. The optical properties of (i) undoped CGW 7070, (ii) 0.5 wt.%, and (iii) 2.0 wt.% Fe_3O_4 doped and reacted CGW 7070, shown in Fig. 2, were used to assess the effect of the doping level on the sample temperature and hydrogen release rate during lamp heating.

3.2.1. *Diffuse versus collimated incidence radiation*

The radiation emitted by an incandescent heat lamp is delivered to the sample as a combination of collimated and diffuse incident radiation [22]. Here, purely diffuse or collimated incident radiations are considered separately. Comparison of the temperature distributions across 1 mm thick undoped and 2 wt.% Fe_3O_4 doped borosilicate glass samples, subjected to collimated and diffuse incident irradiation onto one face for $T_\ell = 2300$ K and exchanging radiation with the surrounding at $T_{sur} = 25\ ^\circ C$, shows that the temperature distribution is relatively uniform across the slab for both diffuse and collimated incident radiation. In addition, increasing the Fe_3O_4 doping level resulted in an increase in the sample temperature at any given time. Indeed, increasing the doping level of the borosilicate glass makes the slab more absorbing in the spectral region between 0.8 and 3.5 μm where more than 80% of the incident radiation from the lamp at $T_\ell = 2300$ K is concentrated.

Moreover, for the same doping level and total incident radiative heat flux, diffuse incidence caused faster and larger temperature rise than collimated incident radiation. It is particularly true for high doping levels. This can be attributed to total internal reflection of radiation coming from within the sample and reaching its surface at angle larger than the critical angle θ_{cr}. This increases the photons' path length and, therefore, the energy deposited in the sample. However, it is absent for normally collimated radiation. The same conclusions were reached for different filament temperatures.

3.2.2. *Effect of lamp emission spectrum*

The effect of the emission spectrum of the incandescent lamp was investigated by considering several values of the filament temperature namely 1700 K, 2300 K, and 2900 K corresponding to peak emission wavelength λ_{max} of 1.7 μm, 1.26 μm, and 1.00 μm, respectively. The irradiance incident onto the sample was kept constant and equal to $q_R = 2\sigma T_f^4 = 2.33\ \mathrm{W/cm^2}$. Fig. 6 shows the evolution of the slab temperature as a function of time for a 1 mm thick sample of CGW 7070 borosilicate slab

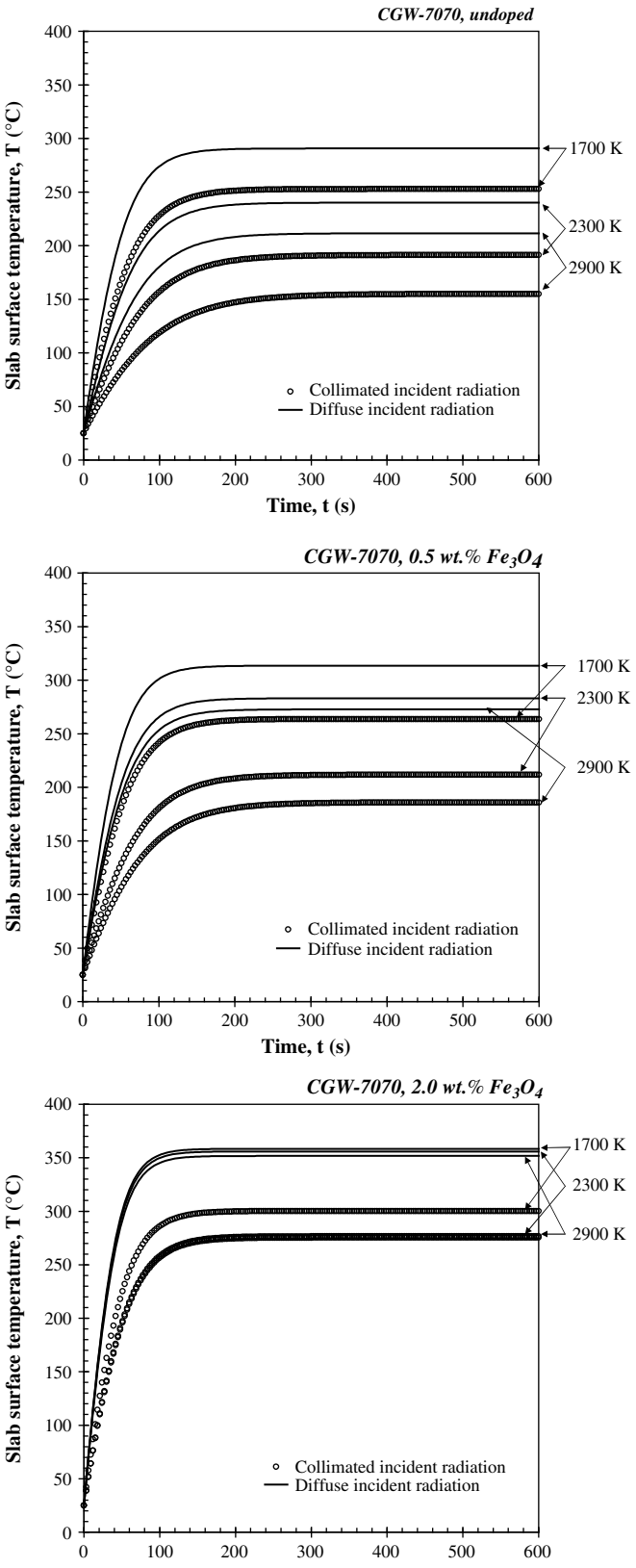

Fig. 6 – Temporal evolution of the temperature of a 1-mm thick sample with different Fe_3O_4 doping level exposed to collimated or diffuse radiation with lamp temperature T_ℓ = 1700, 2300, and 2900 K.

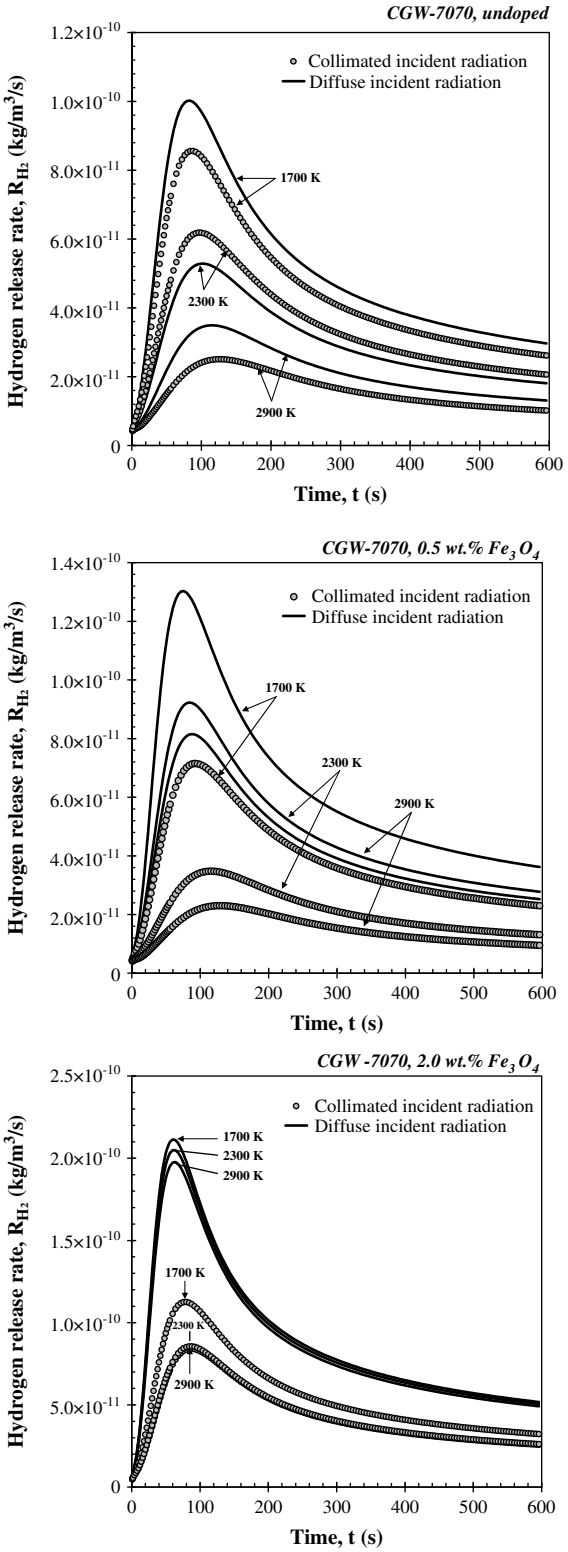

Fig. 7 – Temporal evolution of the H_2 release rate R_{H_2} (t) of a 1-mm thick sample with different Fe_3O_4 doping level exposed to collimated of diffuse lamp radiation with T_ℓ = 1700, 2300, and 2900 K.

with different Fe_3O_4 doping levels exposed to either collimated or diffuse irradiance from incandescent lamp with different filament temperatures. Unlike furnace heating, the doping level has a strong effect on the temporal evolution of the sample temperature. It is also interesting to note that, for a given doping level and incident radiation, the steady-state sample temperature is larger for T_ℓ equal to 1700 K than for 2300 or 2900 K. This is due to the fact that the absorption coefficient is larger for longer wavelengths and becomes significant for wavelengths larger than 2.75 μm (see Fig. 2). Thus, as the lamp temperature increases, the emitted radiation shifts to shorter wavelengths and less energy is absorbed by the sample.

Moreover, the undoped sample reaches 99% of its steady-state temperature of 291 °C after 150 s of exposure to the diffuse irradiance from the lamp at 1700 K. Under the same conditions, the CGW 7070 2.0% Fe_3O_4 doped samples reaches its steady-state temperature of 356 °C after 105 s. Note that if k_λ is set constant and equal to 0.0 for wavelengths between 500 nm and 3.5 μm, the same temperature evolution was observed whether the irradiance was collimated or diffuse for any arbitrary value of the lamp temperature. This suggests that precise knowledge of the optical properties of the sample below the cutoff wavelength is essential for accurate predictions of the evolution of the sample temperature during lamp heating.

Finally, results shown in Fig. 6 for 2.0 wt.% Fe_3O_4 doped samples indicate that the filament temperature has little effect on the sample temperature for diffuse incidence. In other words, for large enough doping level or absorption coefficient, the entire incident heat flux provided in the form of diffuse incident radiation is absorbed by the samples. Then, the sample temperature behaves identically for the three filament temperatures considered and reaches a steady-state value of 350 °C. The same behavior was observed for collimated radiation but for larger Fe_3O_4 doping levels and/or thicker samples. Then, the steady-state temperature reached 270 °C. This should be compared with 350 °C obtained for diffuse incidence and 400 °C for furnace heating for the same total heat input.

Similarly, Fig. 7 shows the hydrogen release rate $R_{H_2}(t)$ as a function of time for a 1 mm thick sample CGW 7070 borosilicate slab with different Fe_3O_4 doping levels exposed to either collimated or diffuse irradiance for different lamp temperatures but identical heat input. It is evident that the hydrogen release rate increases with iron doping level as observed experimentally for lamp heating [7,8]. For high doping level the lamp temperature has no effect on the release rate if the incident radiation is diffuse. Note also that the maximum release rate achieved with lamp heating was 2.1×10^{-10} kg/m^3.s under diffuse incidence. For the same heat input, the maximum release rate from samples directly exposed to furnace radiation ($T_f = 400$ °C) was slightly larger at 3.0×10^{-10} kg/m^3.s.

3.3. *Comparison with experimental data*

Fig. 8a shows the temporal evolution of temperature of a 1-mm thick 2.0 wt.% Fe_3O_4 doped sample during furnace and lamp heating and with and without the silica tube. The same heat input was provided by the two radiation sources emitting diffusely at $T_f = 673$ K and $T_\ell = 1700$ K, respectively. Fig. 8a indicates that the presence of the silica tube significantly reduces the sample heating rate. Indeed, the sample reaches 99% of its steady-state temperature of 400 °C in about 400 and 530 s with silica tube thickness L_t of 1 and 1.5 mm, respectively, as opposed to 60 s when the sample is directly exposed

to furnace radiation. During lamp heating, the sample temperature follows a similar trend as with furnace heating in absence of silica tube but does not exceed 350 °C. This value should be compared with the sample temperature of 472 °C measured experimentally by Rapp [9] (Table III, p. 108) using dilatometry method for the same sample composition. This suggests that, in the experiments, the radiative heat flux delivered by lamp heating was larger than that for furnace heating at 400 °C. This could also be responsible for the observed enhanced hydrogen outgassing.

Fig. 8b compares the hydrogen release rate computed in the present study with the hydrogen partial pressure measured experimentally using a mass spectrometer [8,9]. To enable meaningful comparison, the numerical results were normalized with the maximum release rate ($R_{H_2,max} = 1.3 \times 10^{-10}$ kg/m^2.s) obtained during furnace heating at 400 °C in presence of the silica tube with $L_t = 1.5$ mm. Similarly, experimental data were normalized by the corresponding maximum hydrogen partial pressure of $p_{H_2,max} = 3.41 \times 10^{-7}$ torr (see Fig. 4.4 in Ref. [9]). Fig. 8b indicates that hydrogen release rate is significantly slowed down and reduced in magnitude by the presence of the silica tube. The numerical results are very sensitive to the silica tube thickness L_t, and increasing L_t from 1 to 1.5 mm results in further delay in the peak of the hydrogen release rate.

Overall, the numerical simulations qualitatively predict the trends in the hydrogen release rate observed experimentally for both furnace and lamp heating. First, the peak in the H_2 release rate experimentally occurred around 118 s for furnace heating with silica tube while it was predicted to occur around 200 and 260 s for L_t equal to 1 and 1.5 mm, respectively. Second, for lamp heating, the peak in H_2 release was experimentally observed after 30 s [9] compared with the numerical predictions of 53 and 60 s for furnace heating without silica tube and lamp heating, respectively. Third, the numerical results predicted an increase by a factor of 1.2 to 1.6 in the maximum H_2 release rate from furnace heating with the silica tube ($L_t = 1$ mm) to lamp heating, respectively. Experimentally, a factor 2.9 was observed.

The difference between the experimental results reported by Rapp and Shelby [8,9] and the numerical results can be attributed to (i) multidimensional effects unaccounted for in the simulations, (ii) the difference in the actual emission spectrum of the lamp (Ref. [9], p. 362) compared with the blackbody radiation simulated, (iii) the fact that the total heat input provided experimentally during lamp heating was likely to be larger than that provided during furnace heating as previously discussed, and (iv) the thermophysical and optical properties used differ from that of actual samples.

Note that hydrogen outgassing is as fast and strong for furnace heating without silica tube as it is for lamp heating. This demonstrates that the participation of silica tube in the thermal radiation transfer is mainly responsible for the experimental observations [8]. In other words, for hydrogen outgassing by furnace heating, the samples should be placed in an evacuated container made of a material transparent to the furnace radiation and able to withstand high temperatures such as zinc sulfide (ZnS). Similarly, silica would be the material of choice for the container during lamp heating

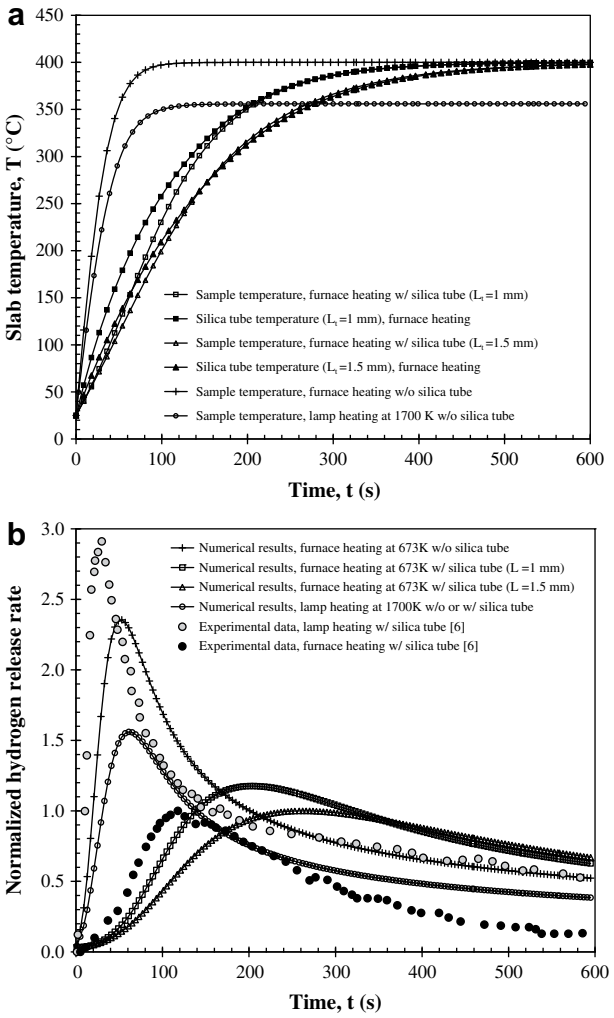

Fig. 8 – Comparison of experimental results [8] with numerical predictions for (a) temperatures and (b) normalized hydrogen release rates for 2.0 wt.% Fe_3O_4 doped CGW 7070 borosilicate sample 1 mm in thickness during furnace heating at $T_f = 400$ °C with samples placed directly in the furnace or inside a silica tube of thickness L_t of 1.0 and 1.5 mm as well as during lamp heating with $T_\ell = 1700$ K.

since it is transparent in the spectral region of emission of the lamp. Then, however, the borosilicate glass needs to be doped and reacted with H_2 to increase its absorptivity in the near-infrared part of the spectrum. A coating reflecting the infrared radiation emitted by the sample could also be deposited inside the containment tube to trap the emitted radiation and increase the heating rate of the sample even further.

Finally, similar analysis can be performed for a bed of hollow glass microspheres. The difference lies in the fact that effective thermal conductivity of the bed must be used and scattering by the hollow microspheres must be accounted for. Heat transfer analysis in packed beds [48–51] can be adapted to predict the temperature inside a bed of HGMs heated by a resistive heater or an incandescent lamp.

4. Conclusion

This paper was concerned with hydrogen release from undoped and Fe_3O_4 doped borosilicate glass by furnace or incandescent lamp heating. The following conclusions were reached:

1. For sample thinner than 10 mm, the temperature is nearly uniform throughout the sample and lump capacitance approach can be used.
2. Unlike during furnace heating, the sample temperature or hydrogen release rate increase with increasing Fe_3O_4 doping levels for lamp heating under both diffuse and collimated incidence. This is attribute to the fact that the furnace emits mainly at wavelengths larger than 3.5 μm where doping does not affect the absorption of borosilicate glass. On the contrary, the doping increases the absorption index below 3.5 μm where the radiation emitted by the incandescent lamp is concentrated.
3. Both the temperature and the hydrogen release rate of doped borosilicate samples are larger for diffuse than for collimated incident radiation from an incandescent lamp thanks to internal reflection within the sample.
4. For large enough doping levels the filament temperature T_ℓ and collimated or diffuse incident radiation has no effect on the temperature rise and on the hydrogen release rate under otherwise identical heat input.
5. Lamp heating takes also advantage of the increase in absorption due to both the Fe_3O_4 doping and its reaction with H_2 upon loading the samples.

Finally, the reported simulations carefully accounting for the spectral behavior of the different glasses uses and using reported thermophysical properties qualitatively predict the experimental observations. For furnace heating, the silica tube absorbs a large fraction of the radiation emitted by the furnace walls around wavelength 4.3 μm. This results in a delay in the temperature rise and a reduction in the sample temperature and the H_2 release rate. On the contrary, the radiation emitted by a heating lamp is concentrated between 0.5 and 3.0 μm and reaches the sample since the silica tube is nearly transparent at wavelengths up to 3.5 μm ($k_\lambda \leq 1 \times 10^{-5}$). However, between 0.8 and 3.2 μm borosilicate does not absorb significantly and needs to be doped. Coincidentally, ferric ions increase the absorption coefficient and also react with H_2 to form ferrous ions which increase the absorption coefficient of the sample by two orders of magnitude (Fig. 2). Thus, doped and reacted samples heat up much faster than undoped ones when exposed to heating lamps. This results in an increase in the H_2 release rate. In brief, experiments under consideration could be qualitatively explained in the framework of conventional diffusion theory. However, the present study does not explain some of the experimental observations [9] including the facts that (1) Ar and Ne are incorporated in the glass much faster with lamp heating than with furnace heating and (2) hydrogen and deuterium are released much faster than helium when samples are exposed to an incandescent lamp.

Acknowledgment

The authors would like to thank Asahi Glass Co. Ltd., Japan for financial support.

Appendix
Supplementary material

Supplementary material can be found, in the online version, at doi: doi:10.1016/j.ijhydene.2009.05.113.

REFERENCES

[1] National Aeronautical and Space Administration Report. Safety standard for hydrogen and hydrogen systems. Report NSS 170.16, February 2, 1997.
[2] Herr M, Lercher JA. Hydrogen storage in microspheres – final report. Energy Technologie; Sept. 9, 2003. Report ET-TN-03-628.
[3] Bouza A, Read CJ, Satyapal S, Milliken J. 2004 Annual DOE hydrogen program review hydrogen storage. U.S. Department of Energy, Energy Efficiency and Renewable Energy, Office of Hydrogen, Fuel Cells and Infrastructure Technologies; 2004.
[4] Riis T, Hagen EF, Vie PJS, Ulleberg Ø. Hydrogen production and storage – R&D priorities and gaps. International Energy Agency – Hydrogen Co-Ordination Group. Hydrogen implementing agreement. Available at: www.iea.org/Textbase/papers/2006/hydrogen.pdf; 2006.
[5] Yartys VA, Lototsky MV. An overview of hydrogen storage methods. In: TN Veziroglu, SY Zaginaichenko, DV Schur, B Baranowski, AP Shpak, VV Skorokhod, and A Kale, editors. Hydrogen materials science and chemistry of carbon nanomaterials. The Netherlands: Kluwer Academic Publishers;2004. pp. 75–104.
[6] Shelby JE, Kenyon BE. Glass membrane for controlled diffusion of gases. US Patent No. 6,231,642 B1, May 15, 2001.
[7] Kenyon BE. Gas solubility and accelerated diffusion in glasses and melts. Master's thesis. Alfred, NY: Alfred University; 1998.
[8] Rapp DB, Shelby JE. Photo-induced hydrogen outgassing of glass. Journal of Non-Crystalline Solids 2004;349:254–9.
[9] Rapp DB. Photo-induced hydrogen outgassing of glass. PhD thesis. Alfred, NY: Alfred University; 2004.
[10] Snyder MJ, Wachtel PB, Hall MM, Shelby JE. Photo-induced hydrogen diffusion in cobalt-doped hollow glass microspheres. Physics and Chemistry of Glasses - European Journal of Glass Science and Technology Part B 2009;50(2): 113–8.
[11] Zhevago NK, Glebov VI. Hydrogen storage in capillary arrays. Energy Conversion and Management 2007;48:1554–9.
[12] Johnston WD, Chelko AJ. Reduction of ions in glass by hydrogen. Journal of American Ceramics Society 1970;53(6): 295–301.
[13] Shelby JE, Vitko Jr J. Hydrogen transport in a machinable glass-ceramic. Journal of Non-Crystalline Solids 1981;45:83–92.
[14] Shelby JE, Vitko Jr J. The reduction of iron in soda-lime-silicate glasses by reaction with hydrogen. Journal of Non-Crystalline Solids 1982;53:155–63.
[15] Faile SP, Roy DM. Dissolution of hydrogen in fused quartz. Journal of American Ceramics Society 1971;54(10):533–4.
[16] Fanderlik. Glass science and technology, vol. 5: optical properties of glass. New York, NY: Elsevier Science; 1983.

[17] Kunc T, Lallemand M, Saulnier JR. Some new developments on coupled radiative–conductive heat transfer in glasses experiments and modeling. International Journal of Heat and Mass Transfer 1984;27(12):2307–19.
[18] Modest MF. Radiative heat transfer. San Diego, CA: Academic Press; 2003.
[19] Asllanaj F, Brige X, Jeandel G. Transient combined radiation and conduction in a one-dimensional non-gray participating medium with anisotropic optical properties subjected to radiative flux at the boundaries. Journal of Quantitative Spectroscopy and Radiative Transfer 2007;107:17–29.
[20] Incropera FP, DeWitt DP. Fundamentals of heat and mass transfer. 4th ed. New York, NY: John Wiley & Sons; 1996.
[21] Siegel R, Howell JR. Thermal radiation heat transfer. 4th ed. New York, NY: Hemisphere Publishing Co; 2002.
[22] Office of Energy Efficiency. Lighting reference guide. Available at: http://%20www.%20oee.%20nrcan.%20gc.%20ca/%20publications/%20equipment/%20lighting/.
[23] Shelby JE. Handbook of gas diffusion in solids and melts. Materials Park, OH: ASM International; 1996.
[24] Dushchenko VP, Kucheruk IM, Berezhnoi PV, Bulyandra AF. Distribution of the irradiance of some "light" infrared sources. Journal of Engineering Physics and Thermophysics 1966;11:161–4.
[25] Kitamura R, Pilon L, Jonasz M. Optical constants of fused quartz from extreme ultraviolet to far infrared at near room temperatures. Applied Optics 2007;46:8118–33.
[26] Assael MJ, Gialou K, Kakosimos K, Metaxa I. Thermal conductivity of reference solid materials. International Journal of Thermophysics 2004;25(2):397–408.
[27] Johnson LF, Hasselman DPH. Thermal diffusivity and conductivity of a carbon fibre-reinforced borosilicate glass. Journal of Material Science 1987;22:3111–7.
[28] Richet P, Bouhifd MA, Courtial P, Téqui C. Configurational heat capacity and entropy of borosilicate melts. Journal of Non-Crystalline Solids 1997;211:271–80.
[29] Bansal NP, Doremus RH. Handbook of glass properties. Orlando, FL: Academic Press, Inc; 1986.
[30] Shelby JE. Helium, deuterium, and neon migration in a common borosilicate glass. Journal of Applied Physics 1974; 45(5):2146–9.
[31] Laska HM, Doremus RH, Jorgensen PJ. Permeation, diffusion, and solubility of deuterium in pyrex glass. Journal of Chemical Physics 1969;50(1):135–7.
[32] Altemose VO. Helium diffusion through glass. Journal of Applied Physics 1961;32(7):1309–16.
[33] De Sousa Meneses D, Gruener G, Malki M, Echegut P. Causal Voigt profile for modeling reflectivity spectra of glasses. Journal of Non-Crystalline Solids 2005;351:124–9.
[34] Low-expansion borosilicate glass. Optical components – optics guide: material properties. Melles Griot Inc; 2007.
[35] Sahba N, Rockett TJ. Infrared absorption coefficients of silica glasses. Journal of the American Ceramic Society 1992;75(1): 209–12.
[36] McMahon HO. Thermal radiation characteristics of some glasses. Journal of American Ceramics Society 1951;34:91–6.
[37] Touloukian YS, DeWitt DP. Thermal properties of matter, radiative, volume 8–thermal radiative properties nonmetallic solids. New York, NY: IFI/Plenum; 1972.
[38] Lohrengel J, Rasper M. Angular emissivity at room temperature and spectral reflectance at near normal incidence of float, borosilicate glass and glass-ceramics. Glass Science and Technology 1996;69:64–74.
[39] Lire DR. CRC handbook of chemistry and physics. 87th ed. Boca Raton, FL: Taylor and Francis; 2006–2007.
[40] Vass CS, Hopp B, Smausz T, Ignácz F. Experiments and numerical calculations for the interpretation of the backside wet etching of fused silica. Thin Solid Films 2004;453–454:121–6.
[41] Drummond DG. The infra-red absorption spectra of quartz and fused silica from 1 to 7.5 μ II – experimental results. Proceedings of the Royal Society of London. Series A, Mathematical and Physical Sciences 1936;153(879):328–39.
[42] Calingaert G, Heron SD, Stair R. Sapphire and other new combustion-chamber window materials. S.A.E. Journal 1936; 39:448–50.
[43] Mamedov RK, Mansurov GM, Dubovikov NI. Optical constants of a chip of fused-silica glass in the IR. Soviet Journal of Optical Technology 1982;49(4):256–8.
[44] Tanaka H, Sawai S, Morimoto K, Hisano K. Evaluation of hemispherical total emissivity for thermal radiation calorimetry. International Journal of Thermophysics 2000;21: 927–40.
[45] Versteeg H, Malalasekra W. An introduction to computational fluid dynamics: the finite volume method. UK: Pearson; 1995.
[46] Viskanta R, Anderson EE. Heat transfer in semitransparent solids. In: Irvine TFJ, Hartnett JP, editors. Advances in heat transfer, vol. 11. New York, London: Academic Press; 1975. p. 317–441.
[47] Hoffman JD. Numerical methods for engineers and scientists. New York, NY: McGraw Hill; 1998.
[48] Chen JC, Churchill SW. Radiant heat transfer in packed beds. AIChE Journal 1963;8:35–41.
[49] Kamiuto K. Correlated radiative transfer in packed-sphere systems. Journal of Quantitative Spectroscopy and Radiative Transfer 1990;43:39–43.
[50] Singh BP, Kaviany M. Modelling radiative heat transfer in packed beds. International Journal of Heat and Mass Transfer 1992;35:1397–405.
[51] Singh BP, Kaviany M. Modelling radiative heat transfer in packed beds. International Journal of Heat and Mass Transfer 1992;35:1397–405.